

SAM Struggles in Concealed Scenes – Empirical Study on “Segment Anything”

Ge-Peng Ji, Deng-Ping Fan, Peng Xu, Ming-Ming Cheng, Bowen Zhou, Luc Van Gool

Abstract—Segmenting anything is a ground-breaking step toward artificial general intelligence, and the Segment Anything Model (SAM) greatly fosters the foundation models for computer vision. We could not be more excited to probe the performance traits of SAM. In particular, exploring situations in which SAM does not perform well is interesting. In this report, we choose three concealed scenes, *i.e.*, camouflaged animals, industrial defects, and medical lesions, to evaluate SAM under unprompted settings. Our main observation is that SAM looks unskilled in concealed scenes.

Index Terms—Segment Anything, SAM, Camouflaged, Concealed Scene Understanding, Concealed Object Segmentation.

1 INTRODUCTION

LARGE models open up new opportunities for AI. In the past few months, there has been a boom in training foundation models on the vast linguistic corpus to produce amazing applications, *e.g.*, ChatGPT¹, GPT-4². Both natural language processing and multimodal learning communities have been revolutionized. Large models’ ability to generalize and emergent makes it easy for users to believe that large models can solve anything.

Last week, the “Segment Anything” [1] project was released, and its Segment Anything Model (SAM) is a large ViT-based model trained on the large visual corpus (SA-1B). This is a ground-breaking step toward artificial general intelligence, as SAM demonstrates promising segmentation capabilities in various scenarios and the great potential of the foundation models for computer vision. Like all computer vision researchers, we cannot wait to probe the performance traits of SAM to help the community to comprehend it further. Moreover, it is interesting to explore the situations in which SAM does not work well.

In this report, we compare SAM quantitatively with cutting-edge models on camouflaged object segmentation task, and present diversified visualization results in three concealed scenes, *i.e.*, camouflaged animals, industrial defects, and medical lesions. Our main observation is that SAM looks not skillful in concealed scenes.

2 EXPERIMENT AND CONCLUSION

We use three frequently-used camouflaged object segmentation (COS) benchmarks to evaluate SAM. In this section, we describe our mask selection strategy (§2.1) and evaluation protocols (§2.2), compare SAM with the state-of-the-art models of COS (§2.3), and provide qualitative visualizations on concealed object segmentation, industrial defect segmentation, and medical lesion segmentation (§2.4).

- Ge-Peng Ji is with the College of Engineering, Computing & Cybernetics, ANU, Canberra, Australia.
- Deng-Ping Fan and Luc Van Gool are with the Computer Vision Lab (CVL), ETH Zurich, Zurich, Switzerland.
- Peng Xu and Bowen Zhou are with the Department of Electronic Engineering, Tsinghua University, Beijing, China.
- Ming-Ming Cheng is with the Nankai University, Tianjin, China.

1. <https://chat.openai.com>
2. <https://openai.com/research/gpt-4>

2.1 Mask Selection Strategy

If under the unprompted setting, SAM generates multiple binary masks and can pop out several potential objects within an input. For a fair evaluation of interesting regions in a specific segmentation task, we take a strategy to select the most appropriate mask based on its ground-truth mask. Formally, given N binary predictions $\{\mathbf{P}_n\}_{n=1}^N$ and the ground-truth \mathbf{G} for an input image, we calculate intersection over union (IoU) scores for each pair to generate a set of evaluation scores $\{\text{IoU}_n\}_{n=1}^N$. We finally select the mask with the highest IoU score from this set.

2.2 Evaluation Protocols

Our protocols are following the standard practice [10].

- **Datasets.** We use three commonly-used COS benchmarks in our experiments, including CAMO [11] (250 samples), COD10K [2] (2,026 samples), and NC4K [12] (4,121 samples).
- **Models.** To ensure a fair comparison with SAM, we choose the current top-performing COS models using transformer architecture, *i.e.*, CamoFormer-P/S [13] and HitNet [14].
- **Metrics.** We use five commonly-used metrics for the evaluation: structure measure (S_α) [15], enhanced-alignment measure (E_ϕ) [16], F-measure (F_β) [17], weighted F-measure (F_β^w) [18], and mean absolute error (M). According to different thresholding strategies, the adaptive/mean/maximum values of F-measure and E-measure are reported. We denote different E_ϕ scores as E_ϕ^{ad} , E_ϕ^{mn} , and E_ϕ^{mx} .

2.3 Quantitative Evaluation

As reported in Table 1, SAM demonstrates significant improvements as model capabilities increase from ViT-B to ViT-L, with an increase in F_β^w score from 0.353 to 0.655. However, the improvement is limited when the model becomes larger, increasing only from 0.655 (ViT-L) to 0.700 (ViT-H). Moreover, we observe that there remains a large gap between SAM even with ViT-H and current top-performing COS models on three benchmarks. For example as presented in Table 1, the difference of E_ϕ^{mx} score between SAM (ViT-H) and CamoFormer-S [13] reaches 13.8%.



Fig. 1. SAM [1] fails to perceive those animals that are visually ‘hidden’ in their natural surroundings. All the samples are from COD10K dataset [2]. The predictions in the third row are generated by the [online demo](#) of SAM.

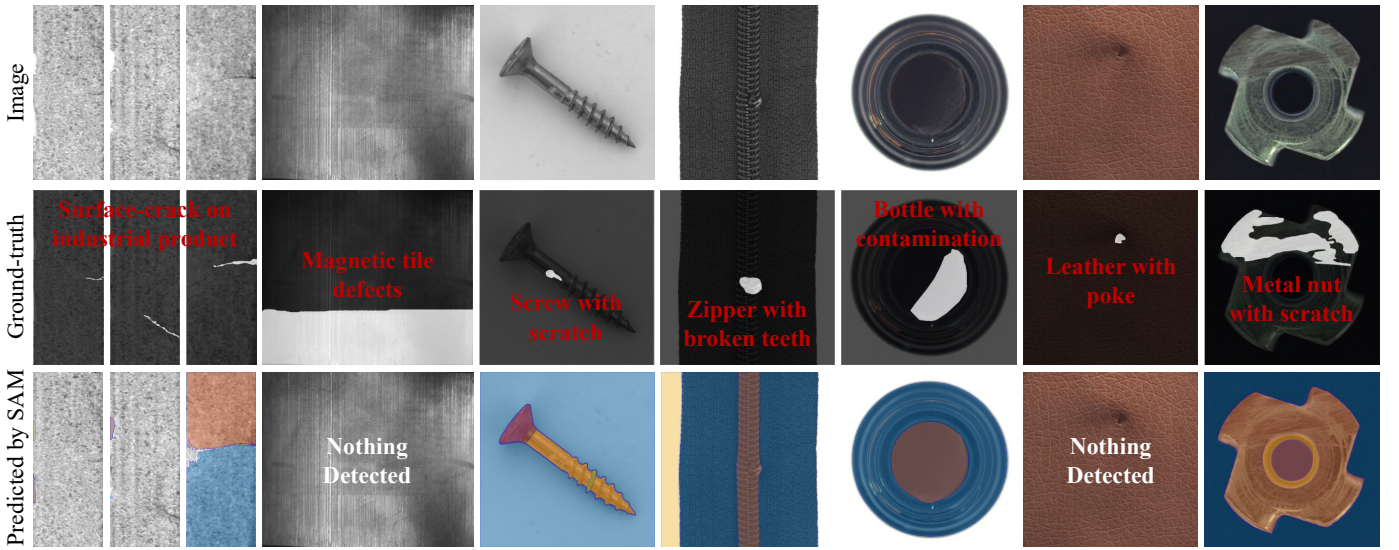


Fig. 2. SAM [1] is unskilled in detecting concealed defects in industrial scenes. These samples are taken from KolektorSDD [3], MagneticTile [4], and MVTecAD [5].

TABLE 1
Quantitative comparison on COD10K [2] dataset. The symbols \uparrow/\downarrow indicate that a higher/lower score is better. The highest scores are marked in bold. Δ represents the difference between SAM and the highest score achieved by well-trained COD models.

Model	Pub/Year	Backbone	$S_\alpha \uparrow$	$F_\beta^w \uparrow$	$M \downarrow$	$E_\phi^{ad} \uparrow$	$E_\phi^{mn} \uparrow$	$E_\phi^{mx} \uparrow$	$F_\beta^{ad} \uparrow$	$F_\beta^{mn} \uparrow$	$F_\beta^{mx} \uparrow$
CamoFormer-P [13]	arXiv23	PVTv2-B4 [19]	0.869	0.786	0.023	0.931	0.932	0.939	0.794	0.811	0.829
CamoFormer-S [13]	arXiv23	Swin-B [20]	0.862	0.772	0.024	0.932	0.931	0.941	0.780	0.799	0.818
HitNet [14]	AAAI23	PVTv2-B2 [19]	0.871	0.806	0.023	0.936	0.935	0.938	0.818	0.823	0.838
SAM [1]	arXiv23	ViT-B [21]	0.585	0.353	0.108	0.535	0.533	0.535	0.423	0.422	0.423
		Difference (Δ)	-28.6%	-45.3%	+8.5%	-40.1%	-40.2%	-40.3%	-39.5%	-40.1%	-41.5%
		ViT-L [21]	0.751	0.655	0.065	0.766	0.764	0.766	0.718	0.716	0.718
		Difference (Δ)	-12%	-15.1%	+4.2%	-17%	-17.1%	-17.2%	-10%	-10.7%	-12%
		ViT-H [21]	0.781	0.700	0.054	0.800	0.798	0.800	0.756	0.754	0.756
		Difference (Δ)	-9%	-10.6%	+3.1%	-13.6%	-13.7%	-13.8%	-6.2%	-6.9%	-8.2%

2.4 Qualitative Comparison

We further evaluate SAM on three concealed scenarios, and several interesting findings are as follows.

- **Camouflaged animal.** As depicted in Fig. 1, SAM would miss

those concealed animals in the natural scene. For instance, consider the seahorse in the last column which has highly-consistent patterns such as shape and color, thereby making it challenging for SAM to generate accurate predictions.

- **Industrial defect.** In this scenario, SAM’s behavior is to

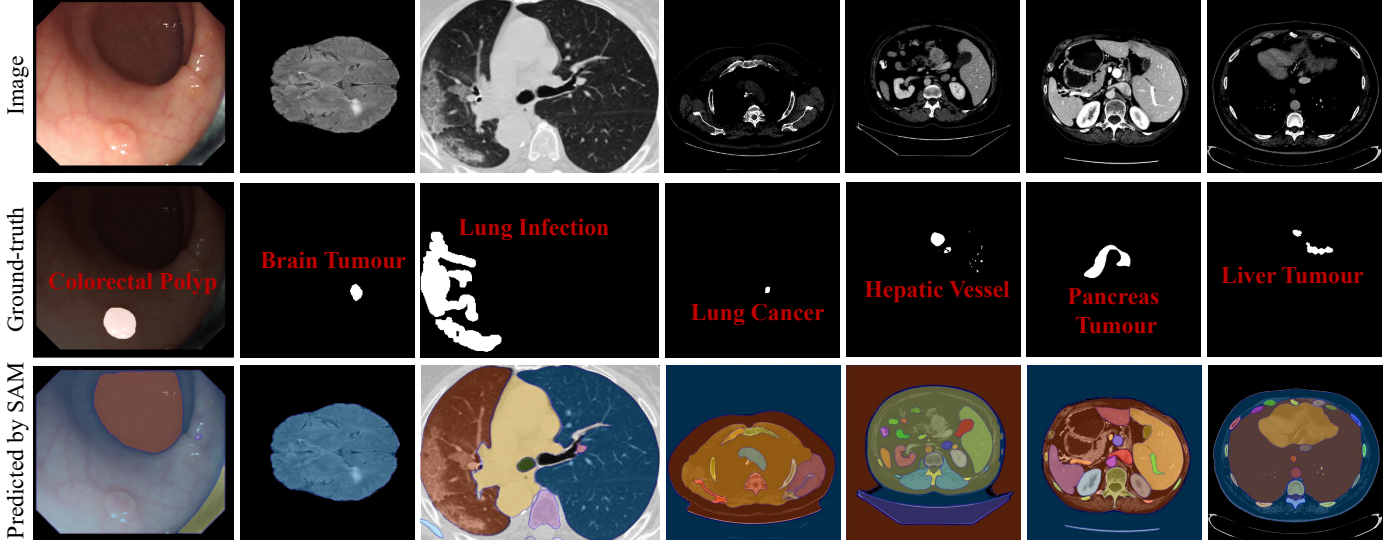


Fig. 3. SAM [1] fails to detect these lesion regions in various medical modalities. These samples cover the RGB colour modality from CVC-300 [6] (1st column); the MRI modality from BraTS2021 [7] (2nd column); the CT modalities from COVID-SemiSeg [8] (3rd column) and MSD [9] (from 4th to 7th columns).

TABLE 2
Quantitative comparison on CAMO [11] dataset. The symbols $\uparrow\downarrow$ denotes that the higher/lower score is better.

Model	Pub/Year	Backbone	$S_\alpha \uparrow$	$F_\beta^w \uparrow$	$M \downarrow$	$E_\phi^{ad} \uparrow$	$E_\phi^{mn} \uparrow$	$E_\phi^{mx} \uparrow$	$F_\beta^{ad} \uparrow$	$F_\beta^{mn} \uparrow$	$F_\beta^{mx} \uparrow$
CamoFormer-P [13]	arXiv ₂₃	PVTv2-B4 [19]	0.872	0.831	0.046	0.931	0.929	0.938	0.853	0.854	0.868
CamoFormer-S [13]	arXiv ₂₃	Swin-B [20]	0.876	0.832	0.043	0.935	0.930	0.938	0.856	0.856	0.871
HitNet [14]	AAAI ₂₃	PVTv2-B2 [19]	0.849	0.809	0.055	0.910	0.906	0.910	0.833	0.831	0.838
SAM [1]	arXiv ₂₃	ViT-B [21]	0.462	0.238	0.219	0.402	0.401	0.402	0.312	0.312	0.312
		Difference (Δ)	-41.4%	-59.4%	+17.6%	-53.3%	-52.9%	-53.6%	-54.4%	-54.4%	-55.9%
		ViT-L [21]	0.630	0.534	0.162	0.628	0.626	0.628	0.617	0.615	0.617
		Difference (Δ)	-24.6%	-29.8%	+11.9%	-30.7%	-30.4%	-31%	-23.9%	-24.1%	-25.4%
		ViT-H [21]	0.677	0.594	0.136	0.682	0.680	0.682	0.670	0.668	0.670
		Difference (Δ)	-19.9%	-23.8%	+9.3%	-25.3%	-25%	-25.6%	-18.6%	-18.8%	-20.1%

TABLE 3
Quantitative comparison on NC4K [12] dataset. The symbols $\uparrow\downarrow$ denotes that the higher/lower score is better.

Model	Pub/Year	Backbone	$S_\alpha \uparrow$	$F_\beta^w \uparrow$	$M \downarrow$	$E_\phi^{ad} \uparrow$	$E_\phi^{mn} \uparrow$	$E_\phi^{mx} \uparrow$	$F_\beta^{ad} \uparrow$	$F_\beta^{mn} \uparrow$	$F_\beta^{mx} \uparrow$
CamoFormer-P [13]	arXiv ₂₃	PVTv2-B4 [19]	0.892	0.847	0.030	0.941	0.939	0.946	0.863	0.868	0.880
CamoFormer-S [13]	arXiv ₂₃	Swin-B [20]	0.888	0.840	0.031	0.941	0.937	0.946	0.857	0.863	0.877
HitNet [14]	AAAI ₂₃	PVTv2-B2 [19]	0.875	0.834	0.037	0.928	0.926	0.929	0.854	0.853	0.863
SAM [1]	arXiv ₂₃	ViT-B [21]	0.544	0.334	0.166	0.494	0.493	0.494	0.403	0.403	0.403
		Difference (Δ)	-34.8%	-51.3%	+13.6%	-44.7%	-44.6%	-45.2%	-46%	-46.5%	-47.7%
		ViT-L [21]	0.728	0.643	0.101	0.735	0.733	0.735	0.706	0.704	0.706
		Difference (Δ)	-16.4%	-20.4%	+7.1%	-20.6%	-20.6%	-21.1%	-15.7%	-16.4%	-17.4%
		ViT-H [21]	0.763	0.696	0.087	0.777	0.775	0.777	0.752	0.750	0.752
		Difference (Δ)	-12.9%	-15.1%	+5.7%	-16.4%	-16.4%	-16.9%	-11.1%	-11.8%	-12.8%

segment individual objects, such as the 3rd, 5th, and 7th columns shown in Fig. 2. Moreover, we observe that SAM is hard to distinguish objective defects from textures, such as leather with a poke in the 6th column.

• **Medical lesion.** As illustrated in 1st column of Fig. 3, we observe that SAM cannot well cope with those medical data with concealed patterns, such as benign colorectal polys that have similar colours to its surrounding tissues. The remaining samples are gray-scale slices from MRI and CT modalities. Although SAM can roughly segment the organ regions since they have clear boundaries, it falls short in recognising amorphous lesion regions, such as cancer, vessel, and tumour.

REFERENCES

- [1] A. Kirillov, E. Mintun, N. Ravi, H. Mao, C. Rolland, L. Gustafson, T. Xiao, S. Whitehead, A. C. Berg, W.-Y. Lo *et al.*, “Segment anything,” *arXiv preprint arXiv:2304.02643*, 2023.
- [2] D.-P. Fan, G.-P. Ji, G. Sun, M.-M. Cheng, J. Shen, and L. Shao, “Camouflaged object detection,” in *IEEE Conf. Comput. Vis. Pattern Recog.*, 2020, pp. 2777–2787.
- [3] D. Tabernik, S. Šela, J. Skvarč, and D. Skočaj, “Segmentation-based deep-learning approach for surface-defect detection,” *J. Intell. Manuf.*, vol. 31, no. 3, pp. 759–776, 2020.
- [4] Y. Huang, C. Qiu, and K. Yuan, “Surface defect saliency of magnetic tile,” *The Visual Computer*, vol. 36, no. 1, pp. 85–96, 2020.
- [5] P. Bergmann, K. Batzner, M. Fauser, D. Sattlegger, and C. Steger, “The mvtac anomaly detection dataset: a comprehensive real-world dataset for unsupervised anomaly detection,” *Int. J. Comput. Vis.*, vol. 129, no. 4, pp. 1038–1059, 2021.

- [6] J. Bernal, J. Sánchez, and F. Vilarino, "Towards automatic polyp detection with a polyp appearance model," *Pattern Recognition*, vol. 45, no. 9, pp. 3166–3182, 2012.
- [7] U. Baid, S. Ghodasara, S. Mohan, M. Bilello, E. Calabrese, E. Colak, K. Farahani, J. Kalpathy-Cramer, F. C. Kitamura, S. Pati *et al.*, "The rsna-asnr-miccai brats 2021 benchmark on brain tumor segmentation and radiogenomic classification," *arXiv preprint arXiv:2107.02314*, 2021.
- [8] D.-P. Fan, T. Zhou, G.-P. Ji, Y. Zhou, G. Chen, H. Fu, J. Shen, and L. Shao, "Inf-net: Automatic covid-19 lung infection segmentation from ct images," *IEEE Trans. Med. Imag.*, vol. 39, no. 8, pp. 2626–2637, 2020.
- [9] M. Antonelli, A. Reinke, S. Bakas, K. Farahani, A. Kopp-Schneider, B. A. Landman, G. Litjens, B. Menze, O. Ronneberger, R. M. Summers *et al.*, "The medical segmentation decathlon," *Nature communications*, vol. 13, no. 1, p. 4128, 2022.
- [10] D.-P. Fan, G.-P. Ji, M.-M. Cheng, and L. Shao, "Concealed object detection," *IEEE Trans. Pattern Anal. Mach. Intell.*, vol. 44, no. 10, pp. 6024–6042, 2022.
- [11] T.-N. Le, T. V. Nguyen, Z. Nie, M.-T. Tran, and A. Sugimoto, "Anabanch network for camouflaged object segmentation," *Comput. Vis. Image Underst.*, vol. 184, pp. 45–56, 2019.
- [12] Y. Lv, J. Zhang, Y. Dai, A. Li, B. Liu, N. Barnes, and D.-P. Fan, "Simultaneously localize, segment and rank the camouflaged objects," in *IEEE Conf. Comput. Vis. Pattern Recog.*, 2021, pp. 11 591–11 601.
- [13] B. Yin, X. Zhang, Q. Hou, B.-Y. Sun, D.-P. Fan, and L. Van Gool, "Camoformer: Masked separable attention for camouflaged object detection," *arXiv preprint arXiv:2212.06570*, 2023.
- [14] X. Hu, D.-P. Fan, X. Qin, H. Dai, W. Ren, Y. Tai, C. Wang, and L. Shao, "High-resolution iterative feedback network for camouflaged object detection," in *AAAI Conf. Art. Intell.*, 2023.
- [15] D.-P. Fan, M.-M. Cheng, Y. Liu, T. Li, and A. Borji, "Structure-measure: A new way to evaluate foreground maps," in *Int. Conf. Comput. Vis.*, 2017, pp. 4548–4557.
- [16] D.-P. Fan, G.-P. Ji, X. Qin, and M.-M. Cheng, "Cognitive vision inspired object segmentation metric and loss function," *SCIENTIA SINICA Informationis*, vol. 6, p. 6, 2021.
- [17] A. Borji, M.-M. Cheng, H. Jiang, and J. Li, "Salient object detection: A benchmark," *IEEE Trans. Image Process.*, vol. 24, no. 12, pp. 5706–5722, 2015.
- [18] R. Margolin, L. Zelnik-Manor, and A. Tal, "How to evaluate foreground maps?" in *IEEE Conf. Comput. Vis. Pattern Recog.*, 2014, pp. 248–255.
- [19] W. Wang, E. Xie, X. Li, D.-P. Fan, K. Song, D. Liang, T. Lu, P. Luo, and L. Shao, "Pvt v2: Improved baselines with pyramid vision transformer," *Computational Visual Media*, vol. 8, no. 3, pp. 415–424, 2022.
- [20] Z. Liu, Y. Lin, Y. Cao, H. Hu, Y. Wei, Z. Zhang, S. Lin, and B. Guo, "Swin transformer: Hierarchical vision transformer using shifted windows," in *Proceedings of the IEEE/CVF international conference on computer vision*, 2021, pp. 10 012–10 022.
- [21] A. Kolesnikov, D. Weissenborn, X. Zhai, T. Unterthiner, M. Dehghani, M. Minderer, G. Heigold, S. Gelly, J. Uszkoreit, and N. Houlsby, "An image is worth 16-16 words: Transformers for image recognition at scale," in *Int. Conf. Learn. Represent.*, 2021.